Preparation and Characterization of Antimony-Doped Tin Dioxide Electrodes. Part 2. XRD and EXAFS Characterization

F. Montilla,[†] E. Morallón,*[,†] A. De Battisti,[‡] A. Benedetti,[§] H. Yamashita,[#] and J. L. Vázquez[†]

Departamento de Química Física, Universidad de Alicante, Apartado de Correos 99, Alicante, Spain E-03080, Dipartimento di Chimica, Università degli Studi di Ferrara, Via Borsari 46, 44100 Ferrara, Italy, Dipartimento Chimica Física, Università Cà Foscari, Calle Larga S. Marta 2137, 30123 Venezia and via Torino 155/b, 30170 Mestre-Venezia, Italy, and Department of Materials Science and Processing, Graduate School of Engineering, Osaka University, 2-1 Yamada-oka, Suita, Osaka 565-0871, Japan

Received: November 14, 2003; In Final Form: February 25, 2004

Several antimony and platinum doped tin dioxide electrodes supported on titanium have been characterized by X-ray diffraction (XRD) and X-ray absorption spectroscopy (EXAFS) techniques. Ti/SnO_2−Sb electrodes show a rutile-type nanostructure with a distorted unit-cell because of the substitution of the Sn(IV) ion by Sb(V). The presence of platinum on the electrode coating modifies the lattice parameters of the SnO_2 cell due to an amorphization of tin oxide layers. The structural modifications on the different electrode after anodic polarization−deactivation have been analyzed.

1. Introduction

Tin dioxide has some interesting properties for different technological applications such as photovoltaic and optoelectronic devices,[1−3] gas sensing systems,[4] or charge storage matrixes.[5,6] The properties of SnO_2 layers for a selected application can be enhanced by the addition of adequate doping atoms, which may increase the conductivity of the layer for its application like transparent electrodes (In, Sb, or F) or may increase the sensitivity of the sensor toward a selected reducing gas. The optimization of these properties demands a good knowledge of the physicochemical and structural characteristics of these layers with respect to either the preparation technique or the doping components.

Tin dioxide layers have been deposited over a titanium support for use as a dimensionally stable anode (DSA) for chlorine evolution[7] or electrochemical destruction of organic compounds.[8−10] For the latter applications, the conductivity of the SnO_2 electrode is usually enhanced by means of the introduction of a doping atom, usually antimony. These electrodes have high overpotential for the oxygen evolution reaction, and therefore, they exhibit high efficiencies in the anodic oxidation of organic compounds.[11]

The main drawback for the use of Ti/SnO_2−Sb electrodes is their short service life in anodic polarization conditions. There are two key interfaces implied in the deactivation mechanism: support|active oxide and active oxide|electrolyte solution. Considering this, several authors have tried to increase the service life of these electrodes by the improvement of the preparation technique,[12] the introduction of a stabilizing component in the layer like platinum or iridium[10,13,14] or the insertion of a layer between the support and the active oxide layer.[15]

Several studies have been performed about the structural properties of tin oxide layers and the effect of the addition of some doping atoms such as antimony,[3,16,17] platinum,[18] palladium, osmium,[19] etc. by X-ray diffraction (XRD). This technique provides information about the long-range structure.

The local structure around a selected atom can be determined by extended X-ray absorption fine structure (EXAFS). This technique has been employed for the analysis of several electrodes supported on titanium (DSA) like IrO_2, RuO_2, or cobalt oxides.[20,21] Tin oxide films have been also characterized with this technique for the study of the local order around the Sn atom[22,23] or the corresponding doping atoms such as titanium,[24] niobium,[25] or antimony.[26]

In the first part of this work, several Ti/SnO_2−Sb electrodes were prepared and characterized from an electrochemical and morphological point of view. The introduction of little amounts of platinum in the layer produces an increase in the electrode service life of several orders of magnitude.[14] In the present work, XRD and EXAFS studies have been performed in order to understand the structural alterations caused in the tin dioxide as a consequence of the addition of dopant atoms (Sb and Pt). Special attention has been paid to the structural modifications on these electrodes as a consequence of the electrochemical deactivation by anodic polarization.

2. Experimental Section

The electrodes of tin dioxide were prepared by thermal decomposition of the salt precursor on a titanium substrate. The salts precursors were $SnCl_4 \cdot 5H_2O$ (Aldrich), $SbCl_3$ (Fluka p.a.), and H_2PtCl_6 in a mixture ethanol (Merck p.a.) + HCl (Merck p.a.). Prior to the deposition process, the Ti support was etched for 1 h in a solution of boiling oxalic acid (10%). Ti/SnO_2−Sb electrodes were prepared using a solution containing 10% $SnCl_4 \cdot 5H_2O$ + 1% $SbCl_3$, and the electrodes containing platinum were prepared by adding to the previous solution a precursor of platinum. Two sets of electrodes were prepared by adding H_2PtCl_6 0.4% in weight (3% atom) and 2.1% in weight (13%

* To whom correspondence should be addressed. E-mail: morallon@ua.es.
[†] Universidad de Alicante.
[‡] Università degli Studi di Ferrara.
[§] Università Cà Foscari.
[#] Osaka University.

10.1021/jp0374814 CCC: $27.50
Published on Web 03/18/2004

atom), respectively. The precursor solution was brushed on a Ti plate ($1 \times 1 \times 0.05$ cm) and the electrode was introduced in an oven at 400 °C for 10 min. This process was repeated 10, 20, and 30 times for attaining different film thicknesses. A final annealing was performed at 600 °C for 1 h. Details about the preparation method were described in a previous paper.[14] Three types of electrodes were manufactured with the following nominal compositions: Ti/SnO_2−Sb(12% atom), Ti/SnO_2−Sb-(12% atom)−Pt(3% atom), and Ti/SnO_2−Sb(12% atom)−Pt-(13% atom). Three electrodes of each composition have been characterized for the structural analysis, and the values obtained have been averaged for the determination of crystallite size and lattice parameters.

X-ray diffraction measurements were performed using a Phillips diffractometer with a PW1050/70 goniometer. A Ni-filtered Cu Kα radiation ($\lambda = 1.541$ Å), a graphite monochromator, and a proportional pulse-height discriminator PW 1711/10 were used. The profile intensities were measured step by step (0.05° in 2θ) for a whole time of 100 s each scan. The diffractograms obtained are the average of 5 scans. The position of the Ti peaks was used as an internal calibration for peak shift.

Cell parameters were calculated by a computer program using the peak position relevant to the Kα1 monochromatic radiation, obtained by fitting the experimental range with a pseudo-Voigt function per peak plus a background line.

Line broadening analysis was performed in order to determine the volume-weighed average crystallite size. The optimized pseudo-Voigt function obtained for each diffraction peak is Fourier transformed and deconvoluted from the instrumental broadening by Stokes' method. Details in the analysis procedure have been given in previous papers.[27,28]

X-ray absorption experiments (EXAFS) were performed at the BL01B1 station of SPring-8. A Si(111) double crystal was used to monochromatize the X-ray beam from the 8 GeV electron storage ring. The absorption spectra were obtained for the different atoms present in the layers (Pt, Sn, and Sb) in the fluorescence mode at room temperature selecting the appropriate ranges of photon energy (K edge for Sn and Sb atoms and L_{III} for platinum). The normalized spectra were obtained by a procedure described in previous literature,[29] and Fourier transform was performed on k^3-weighted EXAFS oscillations over the range of 3−14 $Å^{-1}$ (FT-EXAFS). Several bulk compounds were analyzed in order to have reference spectra. Those compounds were Pt foil, Sn foil, SnO powder, and SnO_2 powder.

Structural parameters of coordination number (CN), bond distance (R), and Debye−Waller factor (σ) obtained from EXAFS analysis have been calculated with the CDXAS26 program.

3. Structural Characterization

Figure 1A shows the X-ray diffraction pattern of a Ti/SnO_2−Sb electrode freshly prepared. In addition to the sharp peaks related to the titanium support, the peak positions agree well with the reflections of SnO_2 cassiterite indicating a rutile-type structure. The peak corresponding to the (200) reflection is masked by the strong Ti(002) peak at $2\theta = 38.4$. No additional peaks appear corresponding to different phases such as antimony oxides.

The pattern for an electrode containing platinum, Ti/SnO_2−Sb−Pt (13% atom), is shown in Figure 1B. In addition to the peaks associated with the rutile structure, peaks corresponding to the presence of the platinum metallic phase can be observed, specifically the reflections corresponding to the (200) and (220) planes. The peak corresponding to the (100) plane of metallic platinum at $2\theta = 39.8$ is masked by the one of the Ti peaks. No other peaks corresponding to other platinum phases can be observed. Similar diffractograms were obtained with the Ti/SnO_2−Sb−Pt(3%) electrodes.

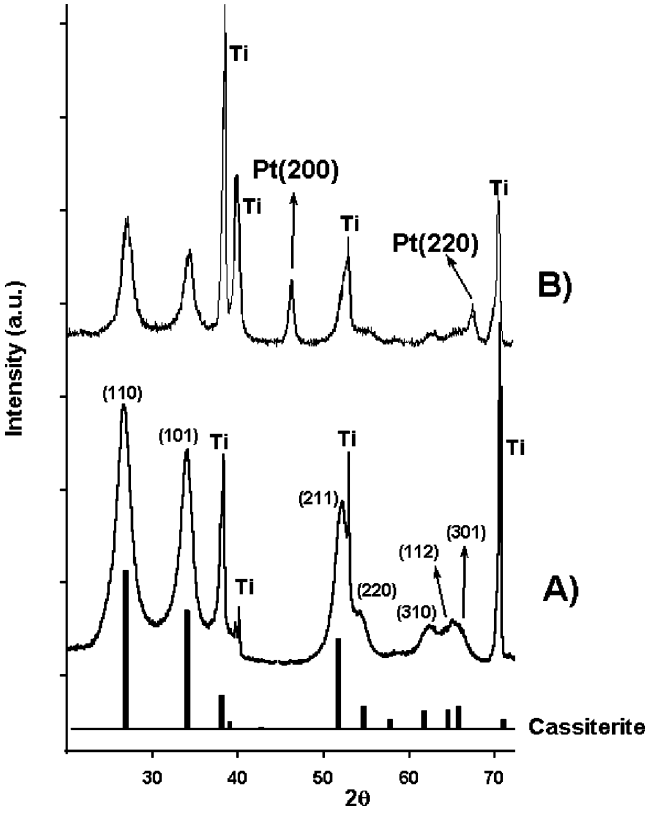

Figure 1. XRD patterns for freshly prepared doped SnO_2 supported on titanium plates: (A) Ti/SnO_2−Sb(12% atom) electrode. (B) Ti/SnO_2−Sb(12% atom)−Pt(13% atom) electrode. The bottom figures show SnO_2 cassiterite and Ti powder standard patterns obtained from the literature (JCPDS-International Center for Diffraction Data).

TABLE 1: Lattice Parameters ($a = b$ and c) and Unit Cell Volume (V) for Different Doped Tin Dioxide Electrodes Calculated from Diffraction Patterns[a]

	lattice parameter		
electrode	a (Å)	c (Å)	V (Å^3)
SnO_2 cassiterite[b]	4.738	3.187	71.54
Ti/SnO_2−Sb	4.725	3.145	70.22
Ti/SnO_2−Sb−Pt (3% atom)	4.703	3.120	69.00
Ti/SnO_2−Sb−Pt (13% atom)	4.703	3.122	69.04

[a] Average values for three electrodes of each composition. [b] JCPS−International Centre for Diffraction Data

The peaks of the rutile phase corresponding to (110), (101), (211), (220), and (310) reflections were deconvoluted and fitted to a pseudo-Voigt function. The relative intensities of the different peaks have been analyzed with the rutile (211) plane being predominant for a greater part of the electrodes, independently of the amount of platinum in the layer (7−9 electrodes analyzed). Chow et al.[30] also found this reflection predominant in antimony doped SnO_2 layers prepared by chemical vapor deposition on quartz disks only in the lowest range of temperature they used (450 °C).

The unit-cell parameters for the doped tin oxides have been calculated using the Bragg's formula and assuming tetragonal tin oxide crystals. Table 1 shows the average values of the lattice parameters obtained for different electrodes ($a = b$ and c). The

TABLE 2: Average Crystallite Sizes Calculated from Different *hkl* Profiles of the SnO_2 Phase and Pt Phase for Doped Tin Dioxide Electrodes[a]

	SnO_2 crystallite size perpendicular to plane (Å)							crystallite size (Å)	
electrode	(110)	(101)	(211)	(220)	(310)	(112)	(301)	SnO_2	Pt
Ti/SnO_2-Sb	*33*	42	48	62	34	53	51	45	
$Ti/SnO_2-Sb-Pt$ (3% atom)	*43*	49	73	*43*	56	67	83	59	58
$Ti/SnO_2-Sb-Pt$ (13% atom)	43	48	65	*35*	77	45	64	54	99

[a] The values in italics indicate the lower crystallite size obtained, for each set of planes. Average values for three electrodes of each composition.

parameters and the volume of the unit-cell obtained are lower than the standard SnO_2. These results can be explained due to the formation of a solid solution between Sn and Sb by the substitution of Sn^{4+} ions (ionic radius 0.83 Å) in the cassiterite structure by Sb^{5+} ions, which have a lower ionic radius (0.74 Å). Taking into account that the amount of Sb is the same in all of the electrodes, the presence of platinum in the layer oxide produces a higher modification on the lattice parameters, which indicates a stronger distortion of the unit-cell.

The level of Sb doping influences the broadening of the diffraction lines and the anisotropy of the widths.[16] However, in all of the electrodes studied in this work, the doping level of Sb is always the same (around 12% atom). Then, the broadening is associated with a modification in the crystallite size. The crystallite size in the samples can be obtained from the analysis of the peak broadening. The diffraction lines are broadened indicating nanosized crystallites in the oxide layer. Table 2 shows the average crystallite size calculated in the perpendicular direction of selected SnO_2 planes. Samples without platinum present crystallite sizes slightly lower than $Ti/SnO_2-Sb-Pt$ electrodes, but differences are not significant. This result is in good agreement with previous results obtained by Labeau et al. in which the SnO_2 crystallite size is slightly affected by the amount of platinum in the deposited oxide layer.[18]

The line broadening of X-ray patterns has an anisotropic character: the peaks of *hh0* planes are broader than the others; that is, the crystallites are smaller in the corresponding directions (see Table 2), which may suggest a layered structure promoted by some oxygen deficiency in the SnO_2 matrix as reported by Grzeta et al.[16]

The platinum crystallite sizes in the $Ti/SnO_2-Sb-Pt$ electrodes have been calculated by means of the broadening analysis of the (200) and (220) reflections. The average values are shown in Table 2. The platinum crystallite size increases as the amount of platinum in the deposited layer increases. The sizes of platinum particles in all of the samples analyzed are in the range 51−117 Å as measured by XRD. Further growing of platinum particles is possibly hindered by the presence of SnO_2 grains.[18]

The local order around a selected atom can be determined by EXAFS spectroscopy. Figure 2 shows the Fourier transforms of EXAFS spectra (FT-EXAFS) obtained in the Sn−K edge absorption for three different standard materials (Sn foil and SnO and SnO_2 powders). Figure 2a shows the FT-EXAFS for a Sn foil where a strong peak at 2.78 Å is observed corresponding to the distance of the first coordination shell of tin atoms (bond length $R_1 = 2.81$ Å). Figure 2b shows the FT-EXAFS spectrum of a SnO powder with a tetragonal litharge structure, where a strong peak at 1.74 Å appears corresponding to the Sn−O first coordination shell (bond length $R_1 = 2.21$ Å). The second peak centered at 3.43 Å corresponds to the Sn−Sn distances of the second coordination shell. Finally, Figure 2c shows the FT-EXAFS spectrum of a SnO_2 powder with a rutile-type structure. The peak in the FT-EXAFS spectrum at 1.59 Å corresponds to the first Sn−O neighbor shell (bond length $R_1 = 2.05$ Å, coordination number $N_1 = 6$), whereas the peak

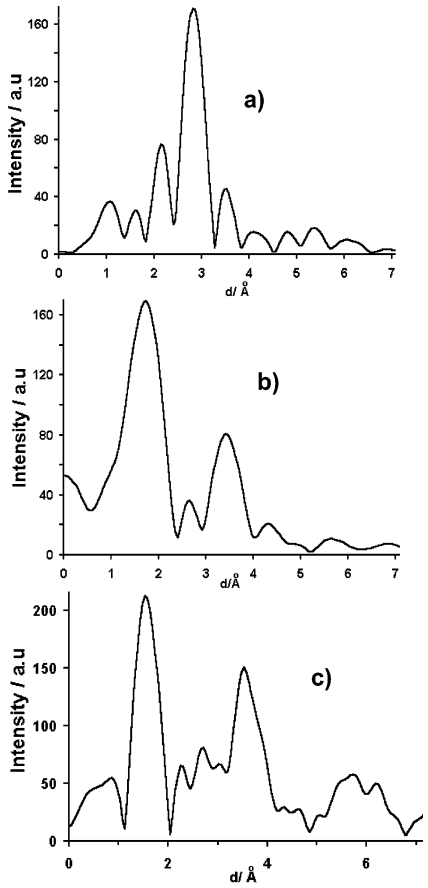

Figure 2. Fourier transform of the EXAFS spectra recorded at the Sn−K edge for several tin-containing standards: (a) tin foil; (b) SnO powder; (c) SnO_2 powder.

centered at 3.53 Å matches with the Sn−Sn coordination shells (2nd shell: $R_2 = 3.19$ Å, $N_2 = 2$ and 3rd shell: $R_3 = 3.71$ Å, $N_3 = 8$).

Figure 3 shows the FT-EXAFS spectra obtained in the Sn−K and in the Sb−K edges for a freshly prepared Ti/SnO_2-Sb electrode and in the Sn−K edge for a deactivated Ti/SnO_2-Sb electrode by anodic polarization. This last spectrum will be discussed later. Figure 3a shows the FT-EXAFS spectrum of a Ti/SnO_2-Sb electrode obtained in the Sn−K edge in which the similar peaks to those obtained with the SnO_2 standard are observed. The main peak appears at 1.59 Å corresponding to the first coordination shell of the Sn−O polyhedron. A second peak appears at 3.55 Å, a similar position obtained for the standard SnO_2 powder. The main difference between the spectra of standard SnO_2 and the Ti/SnO_2-Sb electrode is in the relative intensities between the 1.59 and 3.55 peaks. Whereas in the SnO_2 standard the intensity ratio of the main peaks ($I_{3.55Å}/I_{1.59Å}$) is 0.7, this intensity ratio for the antimony-doped tin dioxide electrode is 0.4. This result indicates a lower crystallite size in the electrodes than in the standard powder. Figure 3b shows a FT-EXAFS spectrum obtained for the same electrode in the

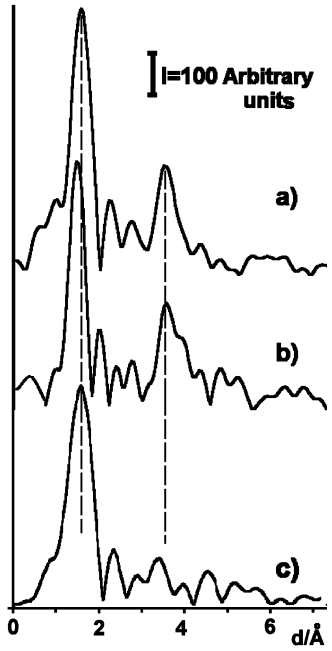

Figure 3. Fourier transform of the EXAFS spectra obtained in the Sn−K edge (a) and in the Sb−K edge (b) for a freshly prepared Ti/SnO_2−Sb(12% atom) electrode and in the Sn−K edge (c) for a Ti/SnO_2−Sb(12% atom) electrode deactivated by anodic polarization.

Sb−K edge in order to check the local environment of the dopant atom in the SnO_2 matrix. The shape of this spectrum is very similar to the Sn−K edge spectrum. This result shows that the chemical environment around a Sb atom is very similar to the local surroundings of a Sn atom in these electrodes, which indicates the substitution of Sn^{IV} atoms by Sb^{V} in the SnO_2 cassiterite structure as proposed by Rockenberger et al.[26] Since the Sb^{V} ionic radius is lower than the Sn^{IV} radius, the cassiterite unit cell is distorted around the dopant atom. In fact, the peak corresponding to the first coordination shell Sb−O appears at 1.48 Å, a lower distance than the Sn−O peak. The position of the peak corresponding to the second coordination shells appears for both Sn and Sb K edges at 3.55 Å with a similar intensity in both cases. Then, only local distortions in the Sb−O polyhedron are produced; however, the long-range structure of SnO_2 is not affected by this substitution, as could also be checked by XRD.

Figure 4 shows the spectra obtained for the Sn−K (a) and Sb−K (b) edges for a freshly prepared Ti/SnO_2−Sb−Pt(13% atom) electrode and the Sn−K edge for a deactivated Ti/SnO_2−Sb−Pt(13% atom) electrode by anodic polarization (c). This last spectrum will be discussed in the next section. The peak for the Sn−O first shell appears at 1.59 Å (Figure 4a), the same position as in electrodes without platinum (Figure 3a). The peak corresponding to the Sb−O first shell appears at a shorter distance (Figure 4b); therefore, the first coordination shell around this atom is similar to that obtained in the electrodes without platinum. The main differences between these spectra and those obtained in the Ti/SnO_2−Sb electrodes are the absence of a clear peak that could be related with a second coordination shell of Sn or Sb. These results indicate a lower short-range order that can be related with a lower crystallite size or an amorphization of the SnO_2 matrix caused by the presence of platinum.

The local environment around the platinum atoms was also checked by EXAFS. Figure 5 shows the spectra obtained in the Pt-L_{III} edge for a freshly prepared Ti/SnO_2−Sb−Pt electrode (solid line) and for a Pt foil (triangle points). The spectrum is

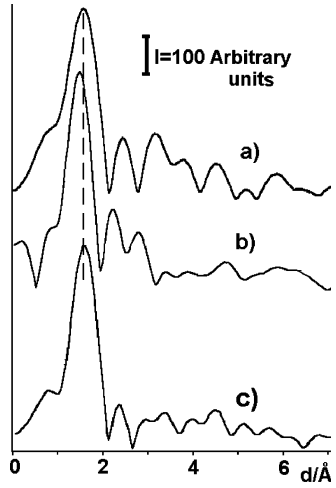

Figure 4. Fourier transform of the EXAFS spectra obtained in the Sn−K edge (a) and in the Sb−K edge (b) for a freshly prepared Ti/SnO_2−Sb(12% atom)−Pt(13% atom) electrode and in the Sn−K edge (c) for a Ti/SnO_2−Sb(12% atom)−Pt(13% atom) electrode deactivated by anodic polarization.

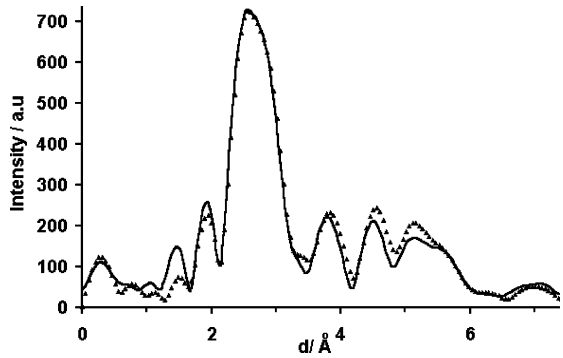

Figure 5. Fourier transform of the EXAFS spectra obtained in the Pt-L_{III} edge: (—) Spectrum for a Ti/SnO_2−Sb(12% atom)−Pt(13% atom) electrode. (triangle points) Spectrum for a platinum foil.

very similar to the spectrum of the Pt foil standard, where a main peak at 2.60 Å can be observed corresponding to the first coordination shell of platinum atoms ($R_1 = 2.74$ Å, $N_C = 12$). The similarity between both spectra suggests the presence of metallic platinum particles dispersed in the oxide layer.

4. Anodic Deactivation of the Electrodes. Structural Modifications.

The service life of a Ti/SnO_2−Sb anode is around 3−10 h at 1 A cm^{-2} in acid media. The introduction of Pt in the oxide layer increases the service life of the electrodes in 1 or 2 orders of magnitude. At the end of the service life tests, the electrodes suffer a complete deactivation for the oxygen evolution reaction. The modifications on these electrodes under the above conditions have been studied by XRD.

Figure 6a shows the diffractograms of a Ti/SnO_2−Sb electrode freshly prepared and after deactivation by anodic polarization. As can be observed in this figure, the oxide layer of the deactivated electrode keeps the rutile-type structure. The intensity ratio of SnO_2/Ti peaks is lower for deactivated electrodes than for fresh electrodes. In addition, there is a higher broadening of the diffraction peaks for the deactivated electrodes. Similar experiments were performed with Ti/SnO_2−Sb−Pt electrodes. Figure 6b shows the diffractogram of a fresh and a deactivated electrode. In these diffractograms, there are no substantial modifications in the shape and intensity of the peaks

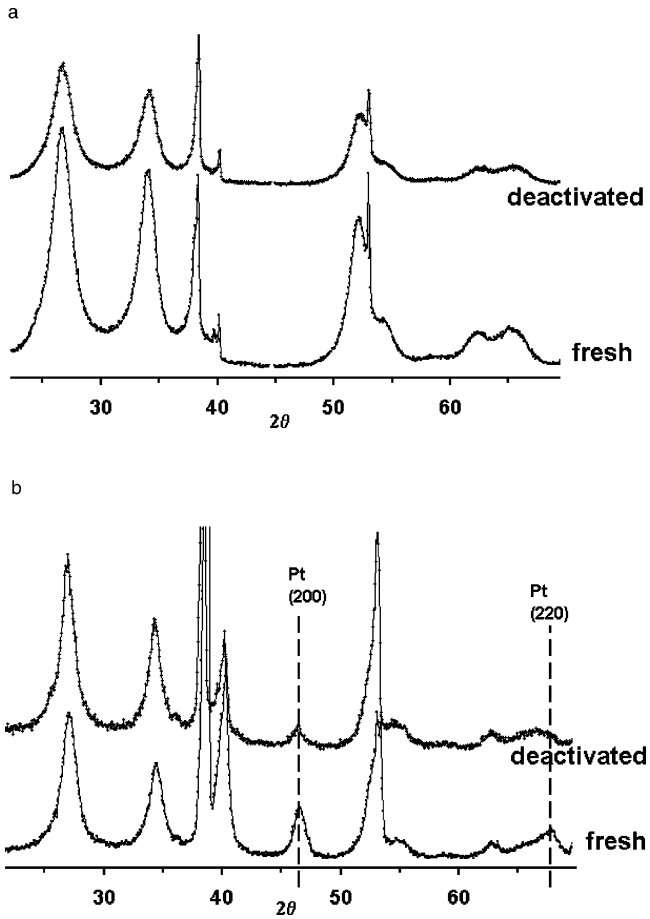

Figure 6. XRD patterns of doped SnO_2 supported on titanium plates: (a) Patterns for Ti/SnO_2-Sb(12% atom) electrodes, freshly prepared (bottom) and after deactivation by anodic polarization (top). (b) Patterns for Ti/SnO_2-Sb(12% atom)−Pt(13% atom) electrodes, freshly prepared (bottom) and after deactivation by anodic polarization (top).

TABLE 3: Lattice Parameters ($a = b$ and c) and Unit Cell Volume (V) of the SnO_2 Phase and Average Crystallite Sizes of the SnO_2 Phase and Pt Phase of Doped Tin Dioxide Electrodes Deactivated by Anodic Polarization[a]

	SnO_2 lattice parameter			crystallite size (Å)	
electrode	a (Å)	c (Å)	V (Å^3)	SnO_2	Pt
Ti/SnO_2-Sb	4.711	3.097	68.73	29	
$Ti/SnO_2-Sb-Pt$(3% atom)	4.697	3.119	68.81	52	46
$Ti/SnO_2-Sb-Pt$(13% atom)	4.694	3.118	68.70	51	73

[a] Average values for three electrodes of each composition.

related with the SnO_2 phase. However, some differences can be observed in the metallic Pt peaks. The relative intensity of these peaks in the deactivated electrodes is lower than in fresh samples. It can be due to either a partial dissolution of the platinum particles or may be related to a change in the microstructure of the platinum phase.

Lattice parameters and average crystallite size of SnO_2 and Pt particles for the deactivated electrodes are shown in Table 3. Deactivated Ti/SnO_2-Sb electrodes have a drop in a and c parameters of the cassiterite cell (evidenced by the decrease in the volume of the unit cell). In contrast, the cell parameters of SnO_2-Sb electrodes containing platinum remain similar to that of the fresh electrodes (only a slight drop of volume can be observed).

The SnO_2 crystallite sizes of a deactivated electrode without platinum is lower (crystallite size 29 Å) than fresh electrodes (crystallite size 45 Å) but, there is almost no modification of the SnO_2 crystallite sizes in electrodes containing Pt. Conversely, a slight reduction in the average size of the platinum particles dispersed in the oxide layer can be observed.

TABLE 4: Structural Parameters (Coordination Number, CN, Bond Distance, R, and Debye−Waller Factor, σ) Obtained from EXAFS Analysis for Fresh and Deactivated Electrodes

electrode	CN	R (Å)	σ^2 (Å^2)
fresh Ti/SnO_2-Sb	5.9	2.06	3.2×10^{-3}
deactivated Ti/SnO_2-Sb	5.5	2.06	2.8×10^{-3}
fresh $Ti/SnO_2-Sb-Pt$(13%atom)	5.4	2.09	3.3×10^{-3}
deactivated $Ti/SnO_2-Sb-Pt$(13%atom)	5.4	2.09	5.1×10^{-4}

The deactivated electrodes were also analyzed by means of X-ray absorption spectroscopy. The FT-EXAFS spectrum of a Ti/SnO_2-Sb deactivated electrode obtained in the Sn−K edge is shown in Figure 3c. The main peak related to the first coordination shell Sn−O appears around 1.59 Å, i.e., the same distance obtained with fresh electrodes. When it is compared to the FT-EXAFS spectrum of a fresh electrode (Figure 3a), the peak corresponding to the second and third coordination shell of the Sn atom centered around 3.55 Å cannot be observed in the FT-EXAFS spectrum of the deactivated Ti/SnO_2-Sb electrode (Figure 3c). This fact is indicative of a reduction in the crystallite size of SnO_2 or the amorphization of the tin oxide matrix as previously confirmed by XRD.

The FT-EXAFS spectrum of a $Ti/SnO_2-Sb-Pt$ deactivated electrode obtained in the Sn−K edge is shown in Figure 4c. No substantial differences can be observed in the Sn−K edge FT-EXAFS spectrum of $Ti/SnO_2-Sb-Pt$ deactivated electrodes (Figure 4c) with respect to the fresh electrode (Figure 4.a), and both are characterized by the absence of second coordination shells around the tin atom.

The Pt-L_{III} edge was analyzed for the $Ti/SnO_2-Sb-Pt$ electrodes, but there is no substantial modification in the FT-EXAFS spectrum of the deactivated electrode with respect to the spectrum of fresh samples. As could be detected by XRD, the crystallite size of the platinum particles remains around 50−70 Å after the electrode deactivation (Table 3). According to Roman-Martinez et al.,[31] who studied PtSn/C catalysts, the platinum particles with a size around 50 Å or higher present a similar structure to the bulk metal.

For all of the electrodes, the structural parameters of coordination number, CN, bond distance, R, and Debye−Waller factor, σ, are listed in Table 4. The coordination number for the first coordination shell has been calculated assuming a coordination number of 6 oxygen atoms to each Sn atom for the SnO_2 standard. In the case of deactivated Ti/SnO_2-Sb electrodes, this CN is lower compared with the freshly prepared electrode indicating that the particle sizes of the SnO_2 have decreased by the deactivation process. However, the coordination number of the SnO_2 for the fresh and deactivated electrodes containing platinum are similar indicating that the particle size in this case remains nearly constant. These results are in agreement with the XRD data.

5. Conclusions

Several doped tin dioxide electrodes supported on titanium have been prepared and their structures have been characterized by XRD and EXAFS. XRD characterization has shown that, in agreement with existing literature, Ti/SnO_2-Sb electrodes present a rutile-type structure with a distorted unit-cell because of the substitution of the Sn^{IV} ion by Sb^{V} in the SnO_2 matrix. EXAFS investigation has shown that the chemical environment

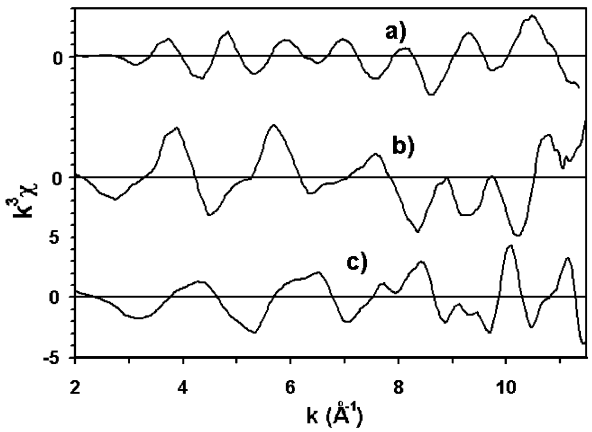

Figure 7. k^3-weighted EXAFS spectra recorded at the Sn−K edge for several tin-containing standards: (a) tin foil; (b) SnO powder; (c) SnO_2 powder.

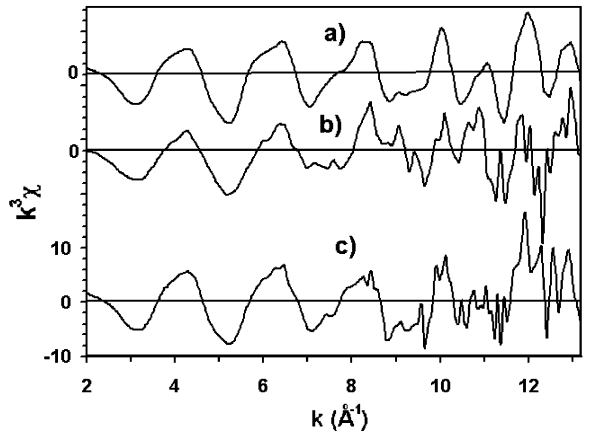

Figure 8. k^3-weighted EXAFS spectra obtained in the Sn−K edge (a) and in the Sb−K edge (b) for a freshly prepared Ti/SnO_2−Sb(12% atom) electrode and in the Sn−K edge (c) for a Ti/SnO_2−Sb(12% atom) electrode deactivated by anodic polarization.

of Sb atoms is very similar to that of the Sn atoms in the antimony-doped tin dioxide electrodes, which serves as a further evidence for the existence of a substitution in solid solution. The introduction of platinum in the layer, maintaining the doping level of antimony constant, causes changes in the lattice parameters of the SnO_2 cell, with partial amorphization of the SnO_2 layer as could be measured by XRD analysis and corroborated by EXAFS. In the absence of any evidence for Pt insertion in the SnO_2 cassiterite structure, this effect may be due to some influence of chloroplatinic acid and of its thermal decomposition products (HCl, Cl_2, and Pt) on the complex kinetics of pyrolysis of the tin and antimony precursors. For instance, the catalytic effect of Pt toward the cracking and combustion of organics in the precursor films during their oxidative pyrolysis could allow a heat release within a shorter time range and the consequent attainment of higher local temperatures. The formation of Pt as a product of H_2PtCl_6 thermolysis, can produce not only HCl, but also Cl_2, favoring the Sb(V) formation. Both of these factors could favor, in turn, the insertion of Sb(V) in the cassiterite lattice and the observed further decrease of lattice parameters. In this case, the appearance of the amorphous component in XRD analysis would witness the hindered growth of crystal phases caused by the higher distortion effects in the lattice shape. As far as the wear resistance of the studied electrodes is concerned, it has been shown that some structural modifications are caused by prolonged anodic polarization. After anodic deactivation, the

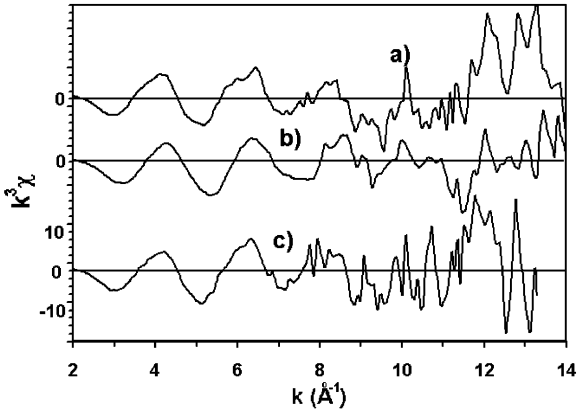

Figure 9. k^3-weighted EXAFS spectra obtained in the Sn−K edge (a) and in the Sb−K edge (b) for a freshly prepared Ti/SnO_2−Sb(12% atom)−Pt(13% atom) electrode and in the Sn−K edge (c) for a Ti/SnO_2−Sb(12% atom)−Pt(13% atom) electrode deactivated by anodic polarization.

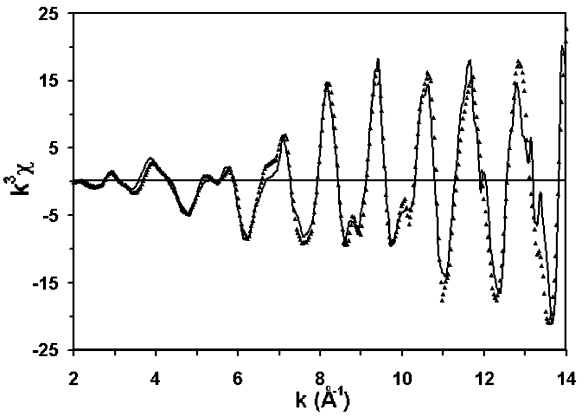

Figure 10. k^3-weighted EXAFS spectra obtained in the Pt-L_{III} edge: (−) Spectrum for a Ti/SnO_2−Sb(12% atom)-Pt(13% atom) electrode. (triangle points) Spectrum for a platinum foil.

electrodes without platinum (Ti/SnO_2−Sb) suffered a modification of the lattice parameters of SnO_2. In addition, a decrease in the tin dioxide crystallite size can be observed.

No substantial modification in the lattice parameter of the cassiterite phase and of its crystallite size has been observed in the case of the deactivated antimony−platinum doped electrodes. Conversely, a reduction of the platinum crystallites appears as a consequence of the anodic polarization. Preferential oxidative attack of larger sized crystallites could be assumed, on the basis of the above evidences.

Acknowledgment. The authors thank Generalitat Valenciana (GV01−313) and Ministerio de Ciencia y Tecnología (MAT 2001−1007) for financial support. The X-ray absorption experiments were performed at the SPring-8 with the approval of the Japan Synchrotron Radiation Research Institute (JASRI) (Proposal Nos. 2002A0613-NX-np, 2001A0018-NX-np, and 2001A0011-NX-np).

Appendix

Figures 7−10 show the k^3-weighted EXAFS spectra corresponding to the FT-EXAFS presented in Figures 2−5, respectively.

References and Notes

(1) Shanthi, S.; Subramanian, C.; Ramasamy, P. *J. Cryst. Growth* **1999**, *197* (4), 858−864.

(2) Abello, L.; Bochu, B.; Gaskov, A.; Koudryavtseva, S.; Lucazeau, G.; Roumyantseva, M. *J. Solid State Chem.* **1998**, *135* (1), 78−85.

(3) Nutz, T.; Haase, M. *J. Phys. Chem. B* **2000**, *104* (35), 8430−8437.

(4) Watson, J.; Ihokura, K.; Coles, G. S. V. *Meas. Sci. Technol.* **1993**, *4* (7), 711−719.

(5) Li, N. C.; Martin, C. R. *J. Electrochem. Soc.* **2001**, *148* (2), A164-A170.

(6) Wu, N. L.; Hwang, J. Y.; Liu, P. Y.; Han, C. Y.; Kuo, S. L.; Liao, K. H.; Lee, M. H.; Wang, S. Y. *J. Electrochem. Soc.* **2001**, *148* (6), A550-A553.

(7) Trasatti, S.; Editor. *Studies in Physical and Theoretical Chemistry, Vol. 11: Electrodes of Conductive Metallic Oxides, Pt. A*.; Elsevier Science Publishers: Amsterdam, The Netherlands, 1980.

(8) Stucki, S.; Kotz, R.; Carcer, B.; Suter, W. *J. Appl. Electrochem.* **1991**, *21* (2), 99−104.

(9) Canizares, P.; Martinez, F.; Diaz, M.; Garcia-Gomez, J.; Rodrigo, M. A. *J. Electrochem. Soc.* **2002**, *149* (8), D118-D124.

(10) Vicent, F.; Morallon, E.; Quijada, C.; Vazquez, J. L.; Aldaz, A.; Cases, F. *J. Appl. Electrochem.* **1998**, *28* (6), 607−612.

(11) Comninellis, C.; Pulgarin, C. *J. Appl. Electrochem.* **1993**, *23* (2), 108−112.

(12) Lipp, L.; Pletcher, D. *Electrochim. Acta* **1997**, *42* (7), 1091−1099.

(13) Chen, G. H.; Chen, X. M.; Yue, P. L. *J. Phys. Chem. B* **2002**, *106* (17), 4364−4369.

(14) Montilla, F.; Morallon, E.; De Battisti, A.; Vazquez, J. L. *J. Phys. Chem. B* **2004**, *108*, 5036.

(15) CorreaLozano, B.; Comninellis, C.; De Battisti, A. *J. Appl. Electrochem.* **1997**, *27* (8), 970−974.

(16) Grzeta, B.; Tkalcec, E.; Goebbert, C.; Takeda, M.; Takahashi, M.; Nomura, K.; Jaksic, M. *J. Phys. Chem. Solids* **2002**, *63* (5), 765−772.

(17) Santos-Pena, J.; Brousse, T.; Sanchez, L.; Morales, J.; Schleich, D. M. *J. Power Sources* **2001**, *97*−*8* 232−234.

(18) Labeau, M.; Gautheron, B.; Cellier, F.; Valletregi, M.; Garcia, E.; Calbet, J. M. G. *J. Solid State Chem.* **1993**, *102* (2), 434−439.

(19) Licciulli, A.; Mazzarelli, S.; De, G.; Siciliano, P.; Vasanelli, L.; Rella, R. *J. Sol−Gel Sci. Technol.* **2001**, *21* (3), 195−201.

(20) Arikawa, T.; Takasu, Y.; Murakami, Y.; Asakura, K.; Iwasawa, Y. *J. Phys. Chem. B* **1998**, *102* (19), 3736−3741.

(21) Totir, D.; Mo, Y. B.; Kim, S.; Antonio, M. R.; Scherson, D. A. *J. Electrochem. Soc.* **2000**, *147* (12), 4594−4597.

(22) Brito, G. E. S.; Briois, V.; Pulcinelli, S. H.; Santilli, C. V. *J. Sol−Gel Sci. Technol.* **1997**, *8* (1−3), 269−274.

(23) Jimenez, V. M.; Espinos, J. P.; Caballero, A.; Contreras, L.; Fernandez, A.; Justo, A.; Gonzalez-Elipe, A. R. *Thin Solid Films* **1999**, *353* (1−2), 113−123.

(24) Oliveira, M. M.; Schnitzler, D. C.; Zarbin, A. J. G. *C. Mater.* **2003**, *15* (9), 1903−1909.

(25) Briois, V.; Pulcinelli, S. H.; Santilli, C. V. *J. Mater. Sci. Lett.* **2001**, *20* (6), 555−557.

(26) Rockenberger, J.; zum Felde, U.; Tischer, M.; Troger, L.; Haase, M.; Weller, H. *J. Chem. Phys.* **2000**, *112* (9), 4296−4304.

(27) Benedetti, A.; Polizzi, S.; Riello, P.; Debattisti, A.; Maldotti, A. *J. Mater. Chem.* **1991**, *1* (4), 511−515.

(28) Nanni, L.; Polizzi, S.; Benedetti, A.; De Battisti, A. *J. Electrochem. Soc.* **1999**, *146* (1), 220−225.

(29) Yamashita, H.; Matsuoka, M.; Tsuji, K.; Shioya, Y.; Anpo, M. J. *J. Phys. Chem.* **1996**, *100* (1), 397−402.

(30) Chow, T. P.; Ghezzo, M.; Baliga, B. J. *J. Electrochem. Soc.* **1982**, *129* (5), 1040−1045.

(31) Roman-Martinez, M. C.; Cazorla-Amoros, D.; Yamashita, H.; de Miguel, S.; Scelza, O. A. *Langmuir* **2000**, *16* (3), 1123−1131.